Chapter 7
Colliding Bodies Optimization

7.1 Introduction

This chapter presents a novel efficient metaheuristic optimization algorithm called colliding bodies optimization (CBO) for optimization. This algorithm is based on one-dimensional collisions between bodies, with each agent solution being considered as the massed object or body. After a collision of two moving bodies having specified masses and velocities, these bodies are separated with new velocities. This collision causes the agents to move toward better positions in the search space. CBO utilizes a simple formulation to find minimum or maximum of functions; also it is independent of parameters [1].

This chapter consists of two parts. In the first part the main algorithm is developed, and three well-studied engineering design problems and two structural design problems taken from the optimization literature are used to investigate the efficiency of the proposed approach [1]. In the second part, the CBO is applied to a number of continuous optimization benchmark problems. These examples include three well-studied space trusses and two planar bridge structures [2].

7.2 Colliding Bodies Optimization

The main goal of this section is to introduce a simple optimization algorithm based on the collision between objects, which is called colliding bodies optimization (CBO).

A. Kaveh, *Advances in Metaheuristic Algorithms for Optimal Design of Structures*,
DOI 10.1007/978-3-319-46173-1_7

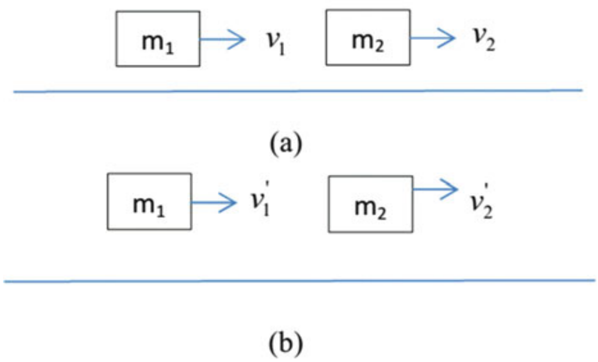

Fig. 7.1 The collision between two bodies. (**a**) Before the collision and (**b**) after the collision [1]

7.2.1 *The Collision Between Two Bodies*

Collisions between bodies are governed by the laws of momentum and energy. When a collision occurs in an isolated system (Fig. 7.1), the total momentum of the system of objects is conserved. Provided that there are no net external forces acting upon the objects, the momentum of all objects before the collision equals the momentum of all objects after the collision.

The conservation of the total momentum demands that the total momentum before the collision is the same as the total momentum after the collision and can be expressed by the following equation:

$$m_1 v_1 + m_2 v_2 = m_1 v_1^{'} + m_2 v_2^{'} \tag{7.1}$$

Likewise, the conservation of the total kinetic energy is expressed as:

$$\frac{1}{2} m_1 {v_1}^2 + \frac{1}{2} m_2 {v_2}^2 = \frac{1}{2} m_1 v_1^{'} 2 + \frac{1}{2} m_2 v_2^{'} 2 + Q \tag{7.2}$$

where v_1 is the initial velocity of the first object before impact, v_2 is the initial velocity of the second object before impact, $v_1^{'}$ is the final velocity of the first object after impact, $v_2^{'}$ is the final velocity of the second object after impact, m_1 is the mass of the first object, m_2 is the mass of the second object, and Q is the loss of kinetic energy due to the impact [3].

The formulas for the velocities after a one-dimensional collision are:

$$v_1^{'} = \frac{(m_1 - \varepsilon m_2) v_1 + (m_2 + \varepsilon m_2) v_2}{m_1 + m_2} \tag{7.3}$$

$$v_2^{'} = \frac{(m_2 - \varepsilon m_1) v_2 + (m_1 + \varepsilon m_1) v_1}{m_1 + m_2} \tag{7.4}$$

where ε is the coefficient of restitution (COR) of the two colliding bodies, defined as the ratio of relative velocity of separation to relative velocity of approach:

$$\varepsilon = \frac{\left|v_2^{'} - v_1^{'}\right|}{\left|v_2 - v_1\right|} = \frac{v^{'}}{v} \tag{7.5}$$

According to the coefficient of restitution, there are two special cases of any collision as follows:

1) A perfectly elastic collision is defined as the one in which there is no loss of kinetic energy in the collision ($Q = 0 \quad and \quad \varepsilon = 1$). In reality, any macroscopic collision between objects will convert some kinetic energy to internal energy and other forms of energy. In this case, after collision, the velocity of separation is high.
2) An inelastic collision is the one in which part of the kinetic energy is changed to some other forms of energy in the collision. Momentum is conserved in inelastic collisions (as it is for elastic collisions), but one cannot track the kinetic energy through the collision since some of it will be converted to other forms of energy. In this case, coefficient of restitution does not equal to one ($Q \neq 0 \quad \& \quad \varepsilon \leq 1$). In this case, after collision the velocity of separation is low.

For the most real objects, the value of ε is between 0 and 1.

7.2.2 The CBO Algorithm

7.2.2.1 Theory

The main objective of the present study is to formulate a new simple and efficient metaheuristic algorithm which is called colliding bodies optimization (CBO). In CBO, each solution candidate X_i containing a number of variables (i.e.,$X_i = \{X_{i,j}\}$) is considered as a colliding body (CB). The massed objects are composed of two main equal groups, i.e., stationary and moving objects, where the moving objects move to follow stationary objects and a collision occurs between pairs of objects. This is done for two purposes: (i) to improve the positions of moving objects and (ii) to push stationary objects toward better positions. After the collision, new positions of colliding bodies are updated based on new velocity by using the collision laws as discussed in the following:

The CBO procedure can briefly be outlined as

1. The initial positions of CBs are determined with random initialization of a population of individuals in the search space:

$$x_i^0 = x_{\min} + rand(x_{\max} - x_{\min}), \quad i = 1, 2, \ldots, n, \tag{7.6}$$

where x_i^0 determines the initial value vector of the ith CB, $x_{\min}$ and $x_{\max}$ are the minimum and the maximum allowable value vectors of variables, *rand* is a random number in the interval [0,1], and n is the number of CBs.

2. The magnitude of the body mass for each CB is defined as:

$$m_k = \frac{\frac{1}{fit(k)}}{\sum_{i=1}^{n} \frac{1}{fit(i)}}, \quad k = 1, 2, \ldots, n \tag{7.7}$$

where $fit(i)$ represents the objective function value of the agent i and n is the population size. It seems that a CB with good values exerts a larger mass than the bad ones. Also, for maximization, the objective function $fit(i)$ will be replaced by $\frac{1}{fit(i)}$.

3. The arrangement of the CBs objective function values is performed in ascending order (Fig. 7.2a). The sorted CBs are equally divided into two groups:

   - The lower half of CBs (stationary CBs); These CBs are good agents which are stationary, and the velocity of these bodies before collision is zero. Thus:

$$v_i = 0, \quad i = 1, \ldots, \frac{n}{2} \tag{7.8}$$

   - The upper half of CBs (moving CBs): These CBs move toward the lower half. Then, according to Fig. 7.2b, the better and worse CBs, i.e., agents with upper fitness value, of each group will collide together. The change of the body position represents the velocity of these bodies before collision as:

$$v_i = x_i - x_{i-\frac{n}{2}}, \quad i = \frac{n}{2} + 1, \ldots, n \tag{7.9}$$

where v_i and x_i are the velocity and position vector of the ith CB in this group, respectively, and $x_{i-\frac{n}{2}}$ is the ith CB pair position of x_i in the previous group.

4. After the collision, the velocities of the colliding bodies in each group are evaluated utilizing Eqs. (7.3) and (7.4) and the velocity before collision. The velocity of each moving CBs after the collision is obtained by:

$$v_i' = \frac{\left(m_i - \varepsilon m_{i-\frac{n}{2}}\right) v_i}{m_i + m_{i-\frac{n}{2}}}, \quad i = \frac{n}{2} + 1, \ldots, n \tag{7.10}$$

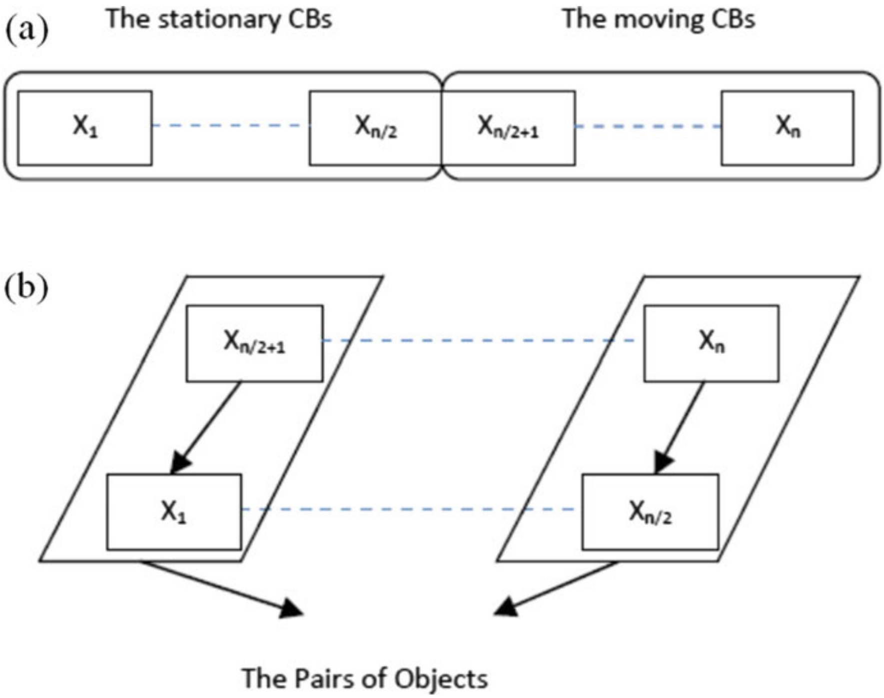

Fig. 7.2 (**a**) CBs sorted in increasing order; (**b**) colliding object pairs [1]

where v_i and $v_i^{'}$ are the velocity of the ith moving CB before and after the collision, respectively; m_i is the mass of the ith CB; and $m_{i-\frac{n}{2}}$ is the mass of the ith CB pair. Also, the velocity of each stationary CB after the collision is:

$$v_i^{'} = \frac{\left(m_{i+\frac{n}{2}} + \varepsilon m_{i+\frac{n}{2}}\right) v_{i+\frac{n}{2}}}{m_i + m_{i+\frac{n}{2}}}, \quad i = 1, \ldots, \frac{n}{2} \tag{7.11}$$

where $v_{i+\frac{n}{2}}$ and $v_i^{'}$ are the velocity of the ith moving CB pair before and the ith stationary CB after the collision, respectively; m_i is the mass of the ith CB; $m_{i+\frac{n}{2}}$ is the mass of the ith moving CB pair; and ε is the value of the COR parameter whose law of variation will be discussed in the next section.

5. New positions of CBs are evaluated using the generated velocities after the collision in position of stationary CBs.
The new positions of each moving CB are:

$$x_i^{new} = x_{i-\frac{n}{2}} + rand \circ v_i^{'}, \quad i = \frac{n}{2} + 1, \ldots, n \tag{7.12}$$

where x_i^{new} and v_i' are the new position and the velocity after the collision of the ith moving CB, respectively, and $x_{i-\frac{n}{2}}$ is the old position of the stationary CB pair. Also, the new positions of stationary CBs are obtained by:

$$x_i^{new} = x_i + rand \circ v_i', \quad i = 1, \ldots, \frac{n}{2} \tag{7.13}$$

where x_i^{new}, x_i, and v_i' are the new position, the old position, and the velocity after the collision of the ith stationary CB, respectively; *rand* is a random vector uniformly distributed in the range (−1,1); and the sign "∘" denotes an element-by-element multiplication.

6. The optimization is repeated from Step 2 until a termination criterion, such as maximum iteration number, is satisfied. It should be noted that a body's status (stationary or moving body) and its numbering are changed in two subsequent iterations.

Apart from the efficiency of the CBO algorithm, which is illustrated in the next section through numerical examples, parameter independency is an important feature that makes CBO superior over other metaheuristic algorithms. Also, the formulation of CBO algorithm does not use the memory which saves the best-so-far solution (i.e., the best position of agents from the previous iterations).

The penalty function approach was used for constraint handling. The fit (i) function corresponds to the effective cost. If optimization constraints are satisfied, there is no penalty; otherwise, the value of penalty is calculated as the ratio between the violation and the allowable limit.

7.2.2.2 The Coefficient of Restitution (COR)

The metaheuristic algorithms have two phases: exploration of the search space and exploitation of the best solutions found. In the metaheuristic algorithm, it is very important to have a suitable balance between the exploration and exploitation. In the optimization process, the exploration should be decreased gradually, while simultaneously exploitation should be increased.

In this chapter, an index is introduced in terms of the coefficient of restitution (COR) to control exploration and exploitation rate. In fact, this index is defined as the ratio of the separation velocity of two agents after collision to approach velocity of two agents before collision. Efficiency of this index will be shown using one numerical example.

In this section, in order to have a general idea about the performance of COR in controlling local and global searches, a benchmark function (Aluffi-Pentini) chosen from Ref. [4] is optimized using the CBO algorithm. Three variants of COR values are considered. Figure 7.3 is prepared to show the positions of the current CBs in the 1st, 50th, and 100th iteration for these cases. These three typical cases result in the following:

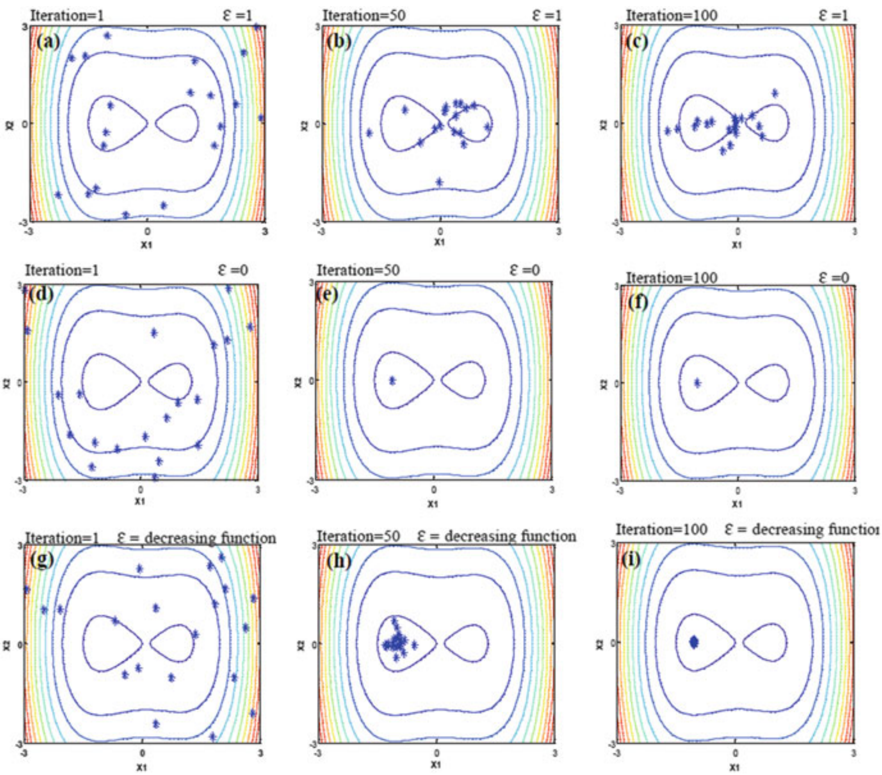

Fig. 7.3 Evolution of the positions of CBs during optimization history for different definitions of the coefficient of restitution (Aluffi-Pentini benchmark function) [1]

1. The perfectly elastic collision: In this case, COR is set equal to unity. It can be seen that in the final iterations, the CBs investigate the entire search space to discover a favorite space (global search).
2. The hypothetical collision: In this case, COR is set equal to zero. It can be seen that in the 50th iterations, the movements of the CBs are limited to very small space in order to provide exploitation (local search). Consequently, the CBs are gathered in a small region of the search space.
3. The inelastic collision: In this case, COR decreases linearly to zero and ε is defined as:

$$\varepsilon = 1 - \frac{iter}{iter_{\max}} \tag{7.14}$$

where *iter* is the actual iteration number and $iter_{max}$ is the maximum number of iterations. It can be seen that the CBs get closer by increasing iteration. In this way a good balance between the global and local search is achieved. Therefore, in the optimization process, COR is considered such as the above equation.

7.2.3 Test Problems and Optimization Results

Three well-studied engineering design problems and two structural design problems taken from the optimization literature are used to investigate the efficiency of the proposed approach. These examples have been previously studied using a variety of other techniques, which are useful to show the validity and effectiveness of the proposed algorithm. In order to assess the effect of the initial population on the final result, these examples are independently optimized with different initial populations.

For engineering design examples, 30 independent runs were performed for CBO, considering 20 individuals and 200 iterations; the corresponding number of function evaluations is 4000. The number of function evaluations set for the GA-based algorithm developed by Coello [5], the PSO-based method developed by He and Wang [6], and the evolution strategies developed by Montes and Coello [7] are 900,000, 200,000, and 25,000, respectively. Similar to CBO, the number of function evaluations for the charged system search algorithm developed by Kaveh and Talatahari [8] is 4000.

In the truss design problems, 20 independent runs were carried out, considering 40 individuals and 400 iterations; hence, the maximum number of structural analyses was 16,000. The CBO algorithm was coded in MATLAB. Structural analysis was performed with the direct stiffness method.

7.2.3.1 Example 1: Design of Welded Beam

As the first example, design optimization of the welded beam shown in Fig. 7.4 is carried out. The welded beam design problem was often utilized to evaluate the performance of different optimization methods. The objective is to find the best set of design variables to minimize the total fabrication cost of the structure subject to shear stress (τ), bending stress (σ), buckling load (Pc), and end deflection (δ) constraints. Assuming $x_1 = h$, $x_2 = l$, $x_3 = t$, and $x_4 = b$ as the design variables, the mathematical formulation of the problem can be expressed as:

Find

$$\{x_1, x_2, x_3, x_4\} \tag{7.15}$$

To minimize

$$\cos t(x) = 1.10471 x_1^2 x_2 + 0.04811 x_3 x_4 (14 + x_2) \tag{7.16}$$

Subjected to

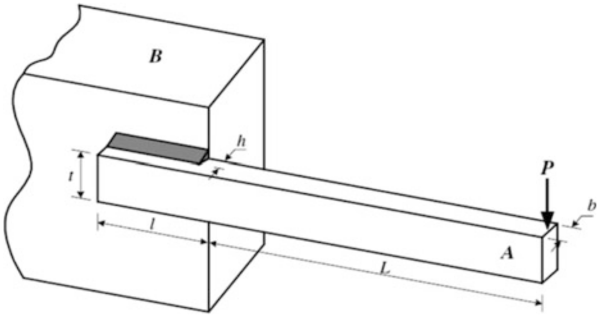

Fig. 7.4 Schematic of the welded beam structure with indication of design variables

$$
\begin{aligned}
g_1(x) &= \tau(x) - \tau_{\max} \leq 0 \\
g_2(x) &= \sigma(x) - \sigma_{\max} \leq 0 \\
g_3(x) &= x_1 - x_4 \leq 0 \\
g_4(x) &= 0.10471x_1^2 + 0.04811x_3x_4(14 + x_2) - 5 \leq 0 \\
g_5(x) &= 0.125 - x_1 \leq 0 \\
g_6(x) &= \delta(x) - \delta_{\max} \leq 0 \\
g_7(x) &= p - p_c(x) \leq 0
\end{aligned}
\tag{7.17}
$$

The bounds on the design variables are:

$$
0.1 \leq x_1 \leq 2, \quad 0.1 \leq x_2 \leq 10, \quad 0.1 \leq x_3 \leq 10, \quad 0.1 \leq x_4 \leq 2 \tag{7.18}
$$

where

$$
\begin{aligned}
&\tau(x) = \sqrt{(\tau')^2 + 2\tau'\tau''\frac{x_2}{2R} + \left(\tau''\right)^2} \\
&\tau' = \frac{P}{\sqrt{2}x_1x_2}\tau'' = \frac{MR}{J}M = P\left(L + \frac{x_2}{2}\right)R = \sqrt{\frac{x_2^2}{4} + \left(\frac{x_1 + x_3}{2}\right)^2} \\
&J = 2\left\{\sqrt{2}x_1x_2\left[\frac{x_2^2}{12} + \left(\frac{x_1+x_3}{2}\right)^2\right]\right\}\sigma(x) = \frac{6PL}{x_4x_3^2}\delta(x) = \frac{4PL^3}{Ex_3^3x_4} \\
&P_c(x) = \frac{4.013\sqrt{E\left(x_3^2x_4^6/36\right)}}{L^2}\left(1 - \frac{x_3}{2L}\sqrt{\frac{E}{4G}}\right)
\end{aligned}
\tag{7.19}
$$

The constants in Eqs. (7.17) and (7.19) are chosen as follows:

$P = 6000$ lb, $L = 14$ in., $E = 30 \times 106$ psi, $G = 12 \times 106$ psi, $\tau_{\max} = 13{,}600$ psi, $\sigma_{\max} = 30{,}000$ psi, and $\delta_{\max} = 0.25$ in.

Radgsdell and Phillips [9] compared optimal results of different optimization methods which were mainly based on mathematical optimization algorithms. Deb [10], Coello [5], and Coello and Montes [11] solved this problem using GA-based methods. Also, He and Wang [6] used effective coevolutionary particle swarm

Table 7.1 Comparison of CBO optimized designs with literature for the welded beam problem

Design variables	Best solution found							
	Ragsdell and Phillips [9]	Deb [10]	Coello [11]	Coello and Montes [11]	He and Wang [6]	Montes and Coello [7]	Kaveh and Talatahari [8]	Present work
x_1 (h)	0.245500	0.248900	0.208800	0.205986	0.202369	0.202369	0.20582	0.205722
x_2 (l)	6.1960000	6.173000	3.420500	3.471328	3.544214	3.544214	3.468109	3.47041
x_3 (t)	8.273000	8.178900	8.997500	9.020224	9.04821	9.04821	9.038024	9.037276
x_4 (b)	0.245500	0.253300	0.210000	0.20648	0.205723	0.205723	0.205723	0.205735
f(x)	1.728024	2.433116	1.748310	1.728226	1.728024	1.728024	1.724866	1.724663

Table 7.2 Statistical results from different optimization methods for the welded beam design problem

Methods	Best result	Average optimized cost	Worst result	Std dev
Ragsdell and Phillips [9]	2.385937	N/A	N/A	N/A
Deb [10]	2.433116	N/A	N/A	N/A
Coello [5]	1.748309	1.771973	1.785835	0.011220
Coello and Montes [11]	1.728226	1.792654	1.993408	0.074713
He and Wang [6]	1.728024	1.748831	1.782143	0.012926
Montes and Coello [7]	1.737300	1.813290	1.994651	0.070500
Kaveh and Talatahari [8]	1.724866	1.739654	1.759479	0.008064
Present work [1]	1.724662	1.725707	1.725059	0.0002437

optimization, Montes and Coello [7] solved this problem utilizing evolution strategies, and Kaveh and Talatahari [8] employed charged system search.

Table 7.1 compares the optimized design and the corresponding cost obtained by CBO with those obtained by other metaheuristic algorithms documented in literature. It can be seen that the best solution obtained by CBO is better than those quoted for the other algorithms. The statistical data on 30 independent runs reported in Table 7.2 also demonstrate the better search ability of CBO with respect to the other algorithms: in fact the best, worst, and average costs and the standard deviation (SD) of the obtained solutions are better than literature. The lowest standard deviation achieved by CBO proves that the present algorithm is more robust than other metaheuristic methods.

7.2.3.2 Test Problem 2: Design of a Pressure Vessel

Design optimization of the cylindrical pressure vessel capped at both ends by hemispherical heads (Fig. 7.5) is considered as the second example. The objective of optimization is to minimize the total manufacturing cost of the vessel based on the combination of welding, material, and forming costs. The vessel is designed for a working pressure of 3000 psi and a minimum volume of 750 ft^3 regarding the provisions of *ASME* boiler and pressure vessel code. Here, the shell and head thicknesses should be multiples of 0.0625 in. The thickness of the shell and head is restricted to 2 in. The shell and head thicknesses must not be $<$1.1 in. and 0.6 in., respectively. The design variables of the problem are x_1 as the shell thickness (T_s), x_2 as the spherical head thickness (T_h), x_3 as the radius of cylindrical shell (R), and x_4 as the shell length (L). The problem formulation is as follows:

Find

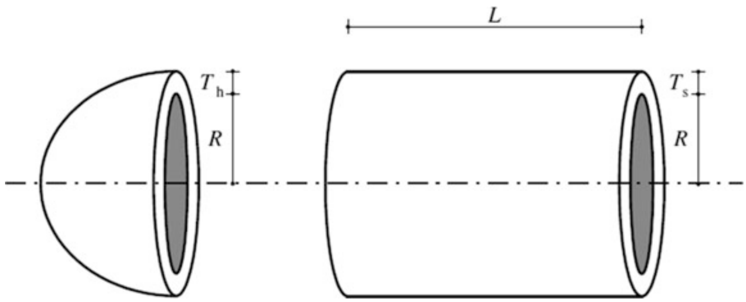

Fig. 7.5 Schematic of the spherical head and cylindrical wall of the pressure vessel with indication of design variables

$$\{x_1, x_2, x_3, x_4\} \tag{7.20}$$

To minimize

$$\cos t(x) = 0.6224x_3x_1x_4 + 1.7781x_3^2x_2 + 3.1611x_1^2x_4 + 19.8621x_3x_1^2 \tag{7.21}$$

Subject to

$$\begin{gathered} g_1(x) = 0.0193x_3 - x_1 \le 0 \\ g_2(x) = 0.00954x_3 - x_2 \le 0 \\ g_3(x) = 750 \times 1728 - \pi x_3^2 x_4 - \frac{4}{3}\pi x_3^3 \le 0 \\ g_4(x) = x_4 - 240 \le 0 \end{gathered} \tag{7.22}$$

The bounds on the design variables are:

$$1.125 \le x_1 \le 2, \quad 0.625 \le x_2 \le 2, \quad 10 \le x_3 \le 240, \quad 10 \le x_4 \le 240 \tag{7.23}$$

It can be seen in Table 7.3 that the present algorithm found the best design overall which is about 3 % lighter than the best known design quoted in literature (5889.911 versus 6059.088 of Ref. [8]). The statistical data reported in Table 7.4 indicate that the standard deviation of CBO optimized solutions is the third lowest among those quoted for the different algorithms compared in this test case. Statistical results given in Table 7.4 indicate that CBO is in general more robust than the other metaheuristic algorithms. However, the worst optimized design and standard deviation found by CBO are higher than for CSS.

7.2.3.3 Test Problem 3: Design of a Tension/Compression Spring

This problem was first described by Belegundu [15] and Arora [16]. It consists of minimizing the weight of a tension/compression spring subject to constraints on

Table 7.3 Comparison of CBO optimized designs with literature for the pressure vessel problem

Methods	X_1 (T_s)	X_2 (T_h)	X_3 (R)	X_4 (L)
Sandgren [12]	1.125000	0.625000	47.70000	117.7010
Kannan and Kramer [13]	1.125000	0.625000	58.29100	43.6900
Deb and Gene [14]	0.937500	0.500000	48.32900	112.6790
Coello [5]	0.812500	0.437500	40.32390	200.0000
Coello and Montes [11]	0.812500	0.437500	42.09739	176.6540
He and Wang [6]	0.812500	0.437500	42.09126	176.7465
Montes and Coello [7]	0.812500	0.437500	42.09808	176.6405
Kaveh and Talatahari [8]	0.812500	0.812500	0.812500	176.572656
Present work [1]	0.779946	0.385560	40.409065	198.76232

Table 7.4 Statistical results from different optimization methods for the pressure vessel problem

Methods	Best result	Average optimized cost	Worst result	Std dev
Sandgren [12]	8129.103	N/A	N/A	N/A
Kannan and Kramer [13]	7198.042	N/A	N/A	N/A
Deb and Gene [14]	6410.381	N/A	N/A	N/A
Coello [5]	6288.744	6293.843	6308.149	7.4133
Coello and Montes [11]	6059.946	6177.253	6469.322	130.9297
He and Wang [6]	6061.077	6147.133	6363.804	86.4545
Montes and Coello [7]	6059.745	6850.004	7332.879	426.0000
Kaveh and Talatahari [8]	6059.088	6067.906	6085.476	10.256
Present work [1]	5889.911	5934.201	6213.006	63.5417

Fig. 7.6 Schematic of the tension/compression spring with indication of design variables

shear stress, surge frequency, and minimum deflection as shown in Fig. 7.6. The design variables are the wire diameter d ($=x_1$), the mean coil diameter D ($=x_2$), and the number of active coils N ($=x_3$). The problem can be stated as follows:

Find

$$\{x_1, x_2, x_3\} \tag{7.24}$$

To minimize

$$\cos t(x) = (x_3 + 2)x_2 x_1^2 \tag{7.25}$$

Subject to

$$
\begin{aligned}
g_1(x) &= 1 - \frac{x_2^3 x_3}{71785 x_1^4} \leq 0 \\
g_2(x) &= \frac{4x_2^2 - x_1 x_2}{12566\left(x_2 x_1^3 - x_1^4\right)} + \frac{1}{5108 x_1^2} - 1 \leq 0 \\
g_3(x) &= 1 - \frac{140.45 x_1}{x_2^2 x_3} \leq 0 \\
g_4(x) &= \frac{x_1 + x_2}{1.5} - 1 \leq 0
\end{aligned}
\tag{7.26}
$$

The bounds on the design variables are:

$$
0.05 \leq x_1 \leq 2, \quad 0.25 \leq x_2 \leq 1.3, \quad 2 \leq x_3 \leq 15, \tag{7.27}
$$

This problem has been solved by Belegundu [15] using eight different mathematical optimization techniques. Arora [16] also solved this problem using a numerical optimization technique called a constraint correction at the constant cost. Coello [5] as well as Coello and Montes [11] solved this problem using GA-based method. Additionally, He and Wang [6] utilized a co-evolutionary particle swarm optimization (CPSO). Recently, Montes and Coello [7] and Kaveh and Talatahari [8] used evolution strategies and the CSS to solve this problem, respectively.

Tables 7.5 and 7.6 compare the best results obtained in this chapter and those of the other researches. Once again, CBO found the best design overall. In fact, the lighter design found by Kaveh and Talatahari in [8] actually violates the first two optimization constraints. The statistical data reported in Table 7.6 show that the standard deviation on optimized cost seen for CBO is fully consistent with literature.

7.2.3.4 Test Problem 4: Weight Minimization of the 120-Bar Truss Dome

The fourth test case solved in this study is the weight minimization problem of the 120-bar truss dome shown in Fig. 7.7. This test case was investigated by Soh and Yang [17] as a configuration optimization problem. It has been solved later as a sizing optimization problem by Lee and Geem [18], Kaveh and Talatahari [8], and Kaveh and Khayatazad [19].

The allowable tensile and compressive stresses are set according to the ASD-AISC (1989) [20] code, as follows:

$$
\begin{cases}
\sigma_i^+ = 0.6F_y & for \sigma_i \geq 0 \\
\sigma_i^- & for \sigma_i \leq 0
\end{cases}
\tag{7.28}
$$

where σ_i^- is calculated according to the slenderness ratio

Table 7.5 Comparison of CBO optimized designs with literature for the tension/compression spring problem

Methods	Optimal design variables			Constraints				
	x_1 (d)	x_2 (D)	x_3 (N)	$g_1(x)$	$g_2(x)$	$g_3(x)$	$g_4(x)$	f(x)
Belegundu [15]	0.050000	0.315900	14.250000	−0.000014	−0.003782	−3.938302	−0.756067	0.0128334
Arora [16]	0.053396	0.399180	9.185400	−0.053396	−0.000018	−4.123832	−0.698283	0.0127303
Coello [5]	0.051480	0.351661	11.632201	−0.002080	−0.000110	−4.026318		0.0127048
Coello and Montes [11]	0.051989	0.363965	10.890522	−0.000013	−0.000021	−4.061338	−0.722698	0.0126810
He and Wang [6]	0.051728	0.357644	11.244543	−0.000845	−1.2600e−05	−4.051300	−0.727090	0.0126747
Montes and Coello [7]	0.051643	0.355360	11.397926	−0.001732	−0.0000567	−4.039301	−0.728664	0.012698
Kaveh and Talatahari [8]	0.051744	0.358532	11.165704	8.78603e−6	0.0011043	−4.063371	−0.726483	0.0126384
Present work [1]	0.051894	0.3616740	11.007846	−3.1073e−4	−1.4189e−5	−4.061846	−0.724287	0.0126697

Table 7.6 Statistical results from different optimization methods for tension/compression string problem

Methods	Best result	Average optimized cost	Worst result	Std dev
Belegundu [15]	0.0128334	N/A	N/A	N/A
Arora [16]	0.0127303	N/A	N/A	N/A
Coello [5]	0.0127048	0.012769	0.012822	3.9390e−5
Coello and Montes [11]	0.0126810	0.0127420	0.012973	5.9000e−5
He and Wang [6]	0.0126747	0.012730	0.012924	5.1985e−5
Montes and Coello [7]	0.012698	0.013461	0.16485	9.6600e−4
Kaveh and Talatahari [8]	0.0126384	0.012852	0.013626	8.3564e−5
Present work [1]	0.126697	0.1272964	0.128808	5.00376e−5

$$\sigma_i^- = \begin{cases} \left[\left(1 - \dfrac{\lambda_i^2}{2C_c^2}\right)F_y\right] \Big/ \left(\dfrac{5}{3} + \dfrac{3\lambda_i}{8C_c} - \dfrac{\lambda_i^3}{8C_c^3}\right) & for \lambda_i < C_c \\ \dfrac{12\pi^2 E}{23\lambda_i^2} & for \lambda_i \geq C_c \end{cases} \tag{7.29}$$

where E is the modulus of elasticity, F_y is the yield stress of steel, C_c is the slenderness ratio (λ_i) dividing the elastic and inelastic buckling regions $\left(C_c = \sqrt{2\pi^2 E/F_y}\right)$, λ_i is the slenderness ratio $\left(\lambda_i = \frac{KL_i}{r_i}\right)$, K is the effective length factor, L_i is the member length, and r_i is the radius of gyration.

The modulus of elasticity is 30,450 ksi (210,000 MPa) and the material density is 0.288 lb/in^3 (7971.810 kg/m^3). The yield stress of steel is taken as 58.0 ksi (400 MPa). On the other hand, the radius of gyration (r_i) is expressed in terms of cross-sectional areas as $r_i = aA_i^{bi}$ [28]. Here, a and b are constants depending on the types of sections adopted for the members such as pipes, angles, and tees. In this example, pipe sections ($a = 0.4993$ and $b = 0.6777$) are adopted for bars. All members of the dome are divided into seven groups, as shown in Fig. 7.7. The dome is considered to be subjected to vertical loads at all the unsupported joints. These are taken as −13.49 kips (60 kN) at node 1, −6.744 kips (30 kN) at nodes 2 through 14, and −2.248 kips (10 kN) at the remaining of the nodes. The minimum cross-sectional area of elements is 0.775 in^2 (cm^2). In this example, four cases of constraints are considered: with stress constraints and no displacement constraints (Case 1), with stress constraints and displacement limitations of ±0.1969 in (5 mm) imposed on all nodes in x and y directions (Case 2), no stress constraints but displacement limitations of ±0.1969 in (5 mm) imposed on all nodes in z directions (Case 3), and all constraints explained above (Case 4). For Case 1 and Case 2, the maximum cross-sectional area is 5.0 in^2 (32.26 cm^2) while for Case 3 and Case 4 is 20.0 in^2 (129.03 cm^2).

Table 7.7 compares the optimization results obtained in this study with previous research presented in literature. It can be seen that CBO always designed the lightest structure except for Cases 3 and 4 where HPSACO converged to a slightly

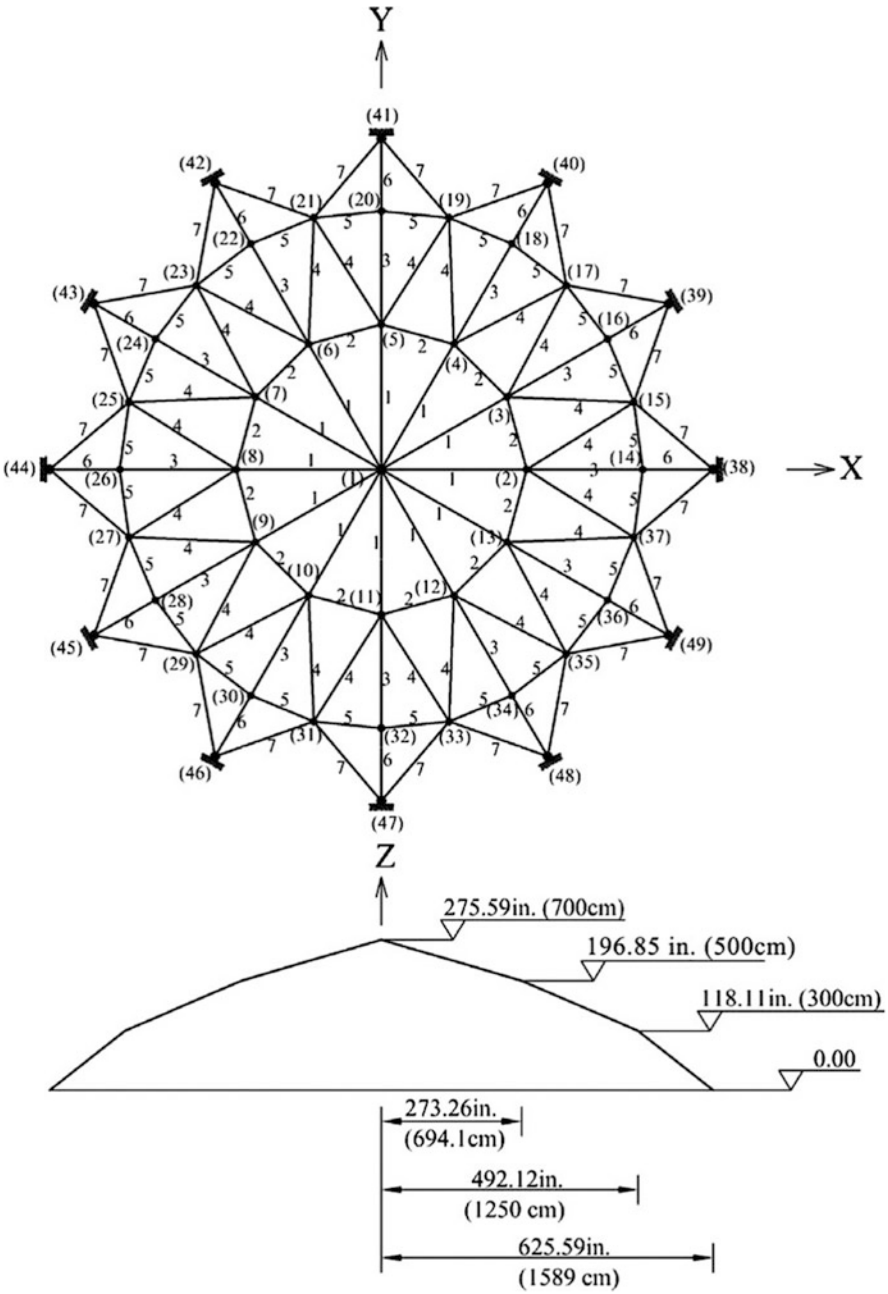

Fig. 7.7 Schematic of the spatial 120-bar dome truss with indication of design variables and main geometric dimensions

Table 7.7 Comparison of CBO optimized designs with literature in the 120-bar dome problem

Element group	Optimal cross-sectional areas (in^2)									
	Case 1					Case 2				
	Kaveh and Khayatazad [19]					Kaveh and Khayatazad [19]				
	PSO	PSOPC	HPSACO	RO	Present work [1]	PSO	PSOPC	HPSACO	RO	Present work [1]
1	3.147	3.235	3.311	3.128	3.1229	15.97	3.083	3.779	3.084	3.0832
2	6.376	3.370	3.438	3.357	3.3538	9.599	3.639	3.377	3.360	3.3526
3	5.957	4.116	4.147	4.114	4.1120	7.467	4.095	4.125	4.093	4.0928
4	4.806	2.784	2.831	2.783	2.7822	2.790	2.765	2.734	2.762	2.7613
5	0.775	0.777	0.775	0.775	0.7750	4.324	1.776	1.609	1.593	1.5918
6	13.798	3.343	3.474	3.302	3.3005	3.294	3.779	3.533	3.294	3.2927
7	2.452	2.454	2.551	2.453	2.4458	2.479	2.438	2.539	2.434	2.4336
Best weight (Ib)	32,432.9	19,618.7	19,491.3	19,476.193	19,454.7	41,052.7	20,681.7	20,078.0	20,071.9	20,064.5
Average weight (Ib)	–	–	–	–	19,466.0	–	–	–	–	20,098.3
Std (Ib)	–	–	–	33.966	7.02	–	–	–	112.135	26.17
	Case 3					Case 4				
1	1.773	2.098	2.034	2.044	2.0660	12.802	3.040	3.095	3.030	3.0284
2	17.635	16.444	15.151	15.665	15.9200	11.765	13.149	14.405	14.806	14.9543
3	7.406	5.613	5.901	5.848	5.6785	5.654	5.646	5.020	5.440	5.4607
4	2.153	2.312	2.254	2.290	2.2987	6.333	3.143	3.352	3.124	3.1214
5	15.232	8.793	9.369	9.001	9.0581	6.963	8.759	8.631	8.021	8.0552
6	19.544	3.629	3.744	3.673	3.6365	6.492	3.758	3.432	3.614	3.3735
7	0.800	1.954	2.104	1.971	1.9320	4.988	2.502	2.499	2.487	2.4899
Weight (lb)	46,893.5	31,776.2	31,670.0	31,733.2	31,724.1	51,986.2	33,481.2	33,248.9	33,317.8	33,286.3
Average weight (Ib)	–	–	–	–	32,162.4	–	–	–	–	33,398.5
Std (Ib)	–	–	–	274.991	240.22	–	–	–	354.333	67.09

lower weight. CBO always completed the optimization process within 16,000 structural analyses (40 agents × 400 optimization iterations), while HPSACO required on average 10,000 analyses (400 optimization iterations) and PSOPC required 125,000 analyses (2500 iterations). The average number of analyses required by the RO algorithm was instead 19,900. Figure 7.8 shows that the convergence rate of CBO is considerably higher than that of PSO and PSOPC.

7.2.3.5 Test Problem 5: Design of Forth Truss Bridge

The last test case was the layout optimization of the Forth Bridge shown in Fig. 7.9a which is a 16 m long and 1 m high truss of infinite span. Because of infinite span, the cross section of the bridge can be modeled as symmetric about the axis joining nodes 10 and 11. Structural symmetry allowed the 37 elements of which the bridge is comprised to be grouped into 16 groups (see Table 7.8); hence, there are 16 independent sizing variables. Nodal coordinates were included as layout variables: x-coordinates of nodes could not vary, while y-coordinates (except those of nodes 1 and 20) were allowed to change between −140 and 140 cm with respect to the initial configuration of Fig. 7.9a. Thus, the optimization problem included also ten layout variables. The cross-sectional areas (sizing variables) could vary between 0.5 and 100 cm^2.

Material properties were set as follows: modulus of elasticity of 210 GPa, allowable stress of 250 MPa, and specific weight of 7.8 t/m^3. The structure is subject to self-weight and concentrated loads shown in Fig. 7.9a.

Table 7.8 compares CBO optimization results with literature. It appears that CBO found the best design overall saving about 1000 kg with respect to the optimum currently reported in literature. Furthermore, the standard deviation on optimized weight observed for CBO in 20 independent optimization runs was lower than for the other metaheuristic optimization algorithms taken as basis of comparison.

The optimized layout of the bridge is shown in Fig. 7.9b. Figure 7.10 compares the convergence behavior of CBO and RO. Although RO was considerably faster in the early optimization iterations, CBO converged to a significantly better design without being trapped in local optima.

7.3 CBO for Optimum Design of Truss Structures with Continuous Variables

This part considers the following: (i) The CBO algorithm is introduced for optimization of continuous problems. (ii) A comprehensive study of sizing optimization for truss structures is presented. The examples are chosen from the literature to verify the effectiveness of the algorithm. These examples are as follows: a

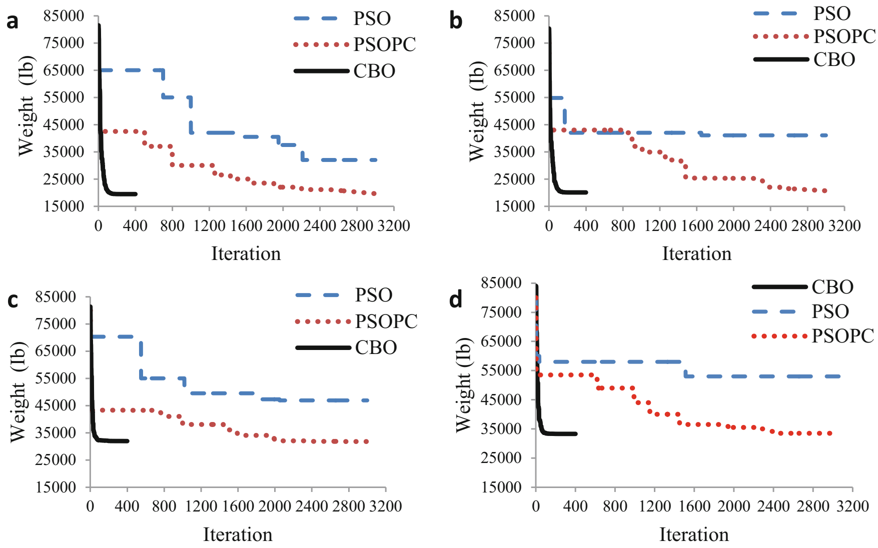

Fig. 7.8 Convergence curves obtained for the different variants of the 120-bar dome problem [2]

25-member spatial truss with 8 design variables, a 72-member spatial truss with 16 design variables, a 582-member space truss tower with 32 design variables, a 37-member plane truss bridge with 16 design variables, and a 68-member plane truss bridge with 4, 8, and 12 design variables. All the structures are optimized for minimum weight with CBO algorithm, and a comparison is carried out in terms of the best optimum solutions and their convergence rates in a predefined number of analyses. The results indicate that the proposed algorithm is very competitive with other state-of-the-art metaheuristic methods.

7.3.1 *Flowchart and CBO Algorithm*

The flowchart of the CBO algorithm is shown in Fig. 7.11. The main steps of CBO algorithm are as follows:

Level 1: Initialization

- **Step 1**: *Initialization*. Initialize an array of CBs with random positions and their associated values of the objective function [Eq. (7.6)].

Level 2: Search

- **Step 1**: *CBs ranking*. Compare the value of the objective function for each CB, and sort them in an increasing order.

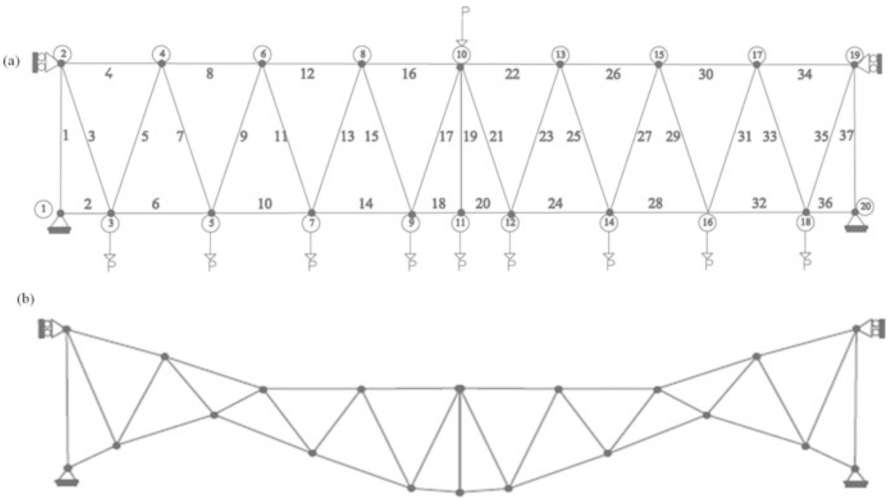

Fig. 7.9 (**a**) Schematic of the Forth Truss Bridge, (**b**) optimized layout of the Forth Bridge [2]

- **Step 2**: *Group creation*. CBs are divided into two equal groups: (i) stationary group and (ii) moving group. Then, the pairs of CB are defined for collision (Fig. 7.2).
- **Step 3**: *Criteria before the collision*. The value of mass and velocity of each CB for each group is evaluated before the collision [Eqs. (7.7)–(7.9)].
- **Step 4**: *Criteria after the collision*. The value velocity of each CB in each groups is evaluated after the collision [Eqs. (7.10) and (7.11)].
- **Step 5**: *CBs updating*. The new position of each CB is calculated [Eqs. (7.13) and Eq. (7.14)].

Level 3: Terminating Criterion Control

- **Step 1**: Repeat search level steps until a terminating criterion is satisfied.

7.3.2 Numerical Examples

In order to assess the effectiveness of the proposed methodology, a number of continuous optimization benchmark problems are examined. These examples include three well-known space trusses and two planar bridge structures. The numbers of design variables for the first to fifth examples are 8, 16, 32, and 26, respectively, and for the last example, 4, 8, and 12 variables are used. Similarly, the numbers of colliding bodies or agents for these examples are considered as

Table 7.8 Comparison of CBO optimization results with literature for the Forth Bridge problem

No	Design variable	Kaveh and Khayatazad [19]			Present work [1]
		BB–BC	PSO	RO	
1	A_1	56.41	25.20	20.54	23.314
2	A_2	58.20	97.60	44.62	36.867
3	A_3, A_5	53.89	35.00	6.37	9.847
4	A_4	60.21	64.30	50.10	49.679
5	A_6	56.27	14.51	30.39	26.563
6	A_7	57.08	37.91	17.61	12.737
7	A_8	49.19	69.85	41.04	37.120
8	A_{10}	48.67	8.76	8.55	1.545
9	A_9, A_{11}	45.43	47.54	33.93	28.35
10	A_{12}	15.14	6.36	0.63	0.891
11	A_{14}	45.31	27.13	26.92	24.110
12	A_{13}	62.91	3.82	23.42	9.112
13	A_{18}	56.77	50.82	42.06	29.071
14	A_{15}, A_{17}	46.66	2.70	2.01	8.222
15	A_{16}	57.95	5.46	8.51	8.715
16	A_{19}	54.99	17.62	1.27	2.107
17	Δy_2, Δy_{19}	6.89	140	70.88	11.093
18	Δy_3, Δy_{18}	17.74	139.65	64.88	50.352
19	Δy_4, Δy_{17}	1.81	117.59	−6.99	−50.529
20	Δy_5, Δy_{16}	23.57	139.70	128.31	119.315
21	Δy_6, Δy_{15}	3.22	−16.51	−64.24	−124.378
22	Δy_7, Δy_{14}	5.85	139.06	139.29	34.219
23	Δy_8, Δy_{13}	4.01	−127.74	−109.62	−120.867
24	Δy_9, Δy_{12}	10.52	−81.03	21.82	−41.323
25	Δy_{10}	−25.99	60.16	−55.09	−115.609
26	Δy_{11}	2.74	−139.97	2.29	−54.590
Best weight (kg)		37,132.3	20,591.9	11,215.7	10,250.9
Average weight (kg)		40,154.1	25,269.3	11,969.2	11,112.63
Std (kg)		1235.4	2323.7	545.5	522.54

Fig. 7.10 Convergence curves obtained in the Forth Bridge problem [2]

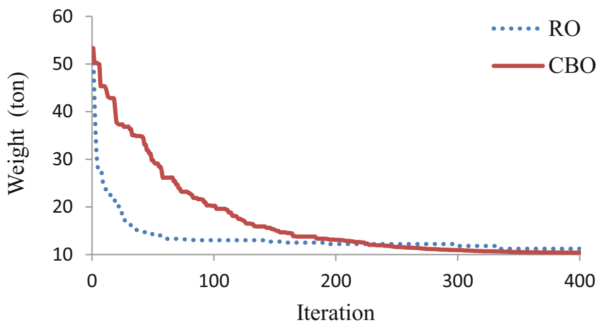

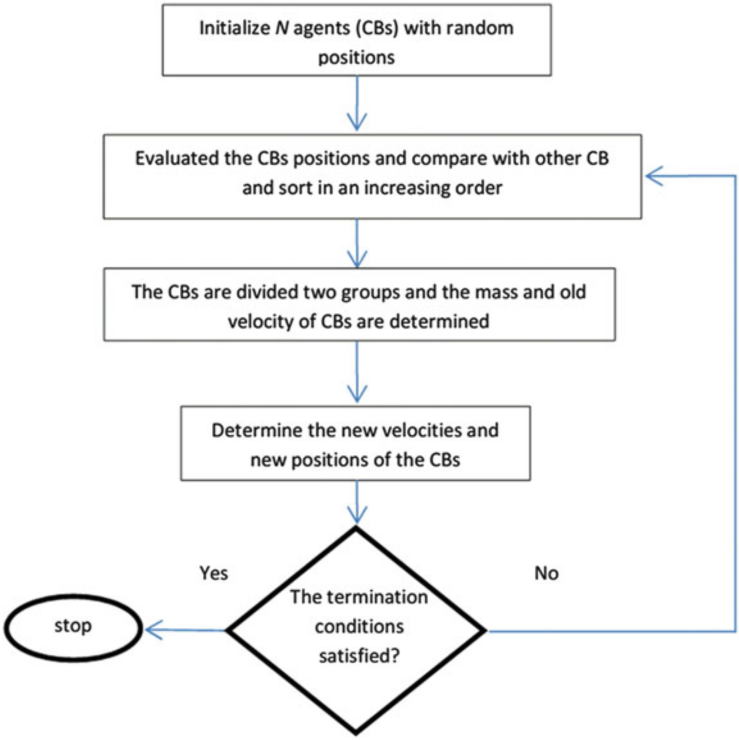

Fig. 7.11 The flowchart of the CBO [2]

30, 40, 50, 40, and 20, respectively. For all of these examples, the maximum number of iteration is considered as 400. The algorithm and the direct stiffness method for the analysis of truss structures are coded in MATLAB software.

For the sake of simplicity and to be fair in comparisons, the penalty approach is used for the constraint handling. The constrained objective function can formally be stated as follows:

$$Mer(X) = f(X) \times f_{penalty}(X) = f(X) \times \left(1 + \varepsilon_1 \sum_{i=1}^{ni} \max(0, g_i(x))\right)^{\varepsilon_2} \tag{7.30}$$

where X is the vector of design variables, g_i is the ith constraint from n_i inequality constraints ($g_i(X) \leq 0$, $i = 1, 2, \ldots, n_i$), $Mer(X)$ is the merit function, $f(X)$ is the weight of structure, and $f_{penalty}(X)$ is the penalty function which results from the violations of the constraints corresponding to the response of the structure. The parameters ε_1 and ε_2 are selected considering the exploration and the exploitation rate of the search space. In this study, ε_1 is selected as unity and ε_2 is taken as 1.5 at the start and linearly increases to 6.

7.3.2.1 A 25-Bar Spatial Truss

Size optimization of the 25-bar planar truss shown in Fig. 7.12 is considered. This is a well-known problem in the field of weight optimization of the structures. In this example, the material density is considered as 0.1 lb/in^3 (2767.990 kg/m^3), and the modulus of elasticity is taken as 10,000 ksi (68,950 MPa). Table 7.9 shows the two load cases for this example. The structure includes 25 members, which are divided into eight groups, as follows: (1) A_1, (2) A_2–A_5, (3) A_6–A_9, (4) A_{10}–A_{11}, (5) A_{12}–A_{13}, (6) A_{14}–A_{17}, (7) A_{18}–A_{21}, and (8) A_{22}–A_{25}.

Maximum displacement limitations of ±0.35 in (8.89 mm) are imposed on every node in every direction, and the axial stress constraints vary for each group as shown in Table 7.10. The range of the cross-sectional areas varies from 0.01 to 3.4 in^2 (0.6452–21.94 cm^2).

By the use of the proposed algorithm, this optimization problem is solved, and Table 7.11 shows the obtained optimal design of CBO, which is compared with GA [21], PSO [22], HS [6], and RO [19]. The best weight of the CBO is 544.310 lb, which is slightly improved compared to other algorithms. It is evident in Table 7.11 that the number of analyses and standard deviation of 20 independent runs for the CBO are 9090 and 0.294 lb, respectively, which are much less than the other optimization algorithms. Figure 7.13 provides the convergence diagram of the CBO in 400 iterations.

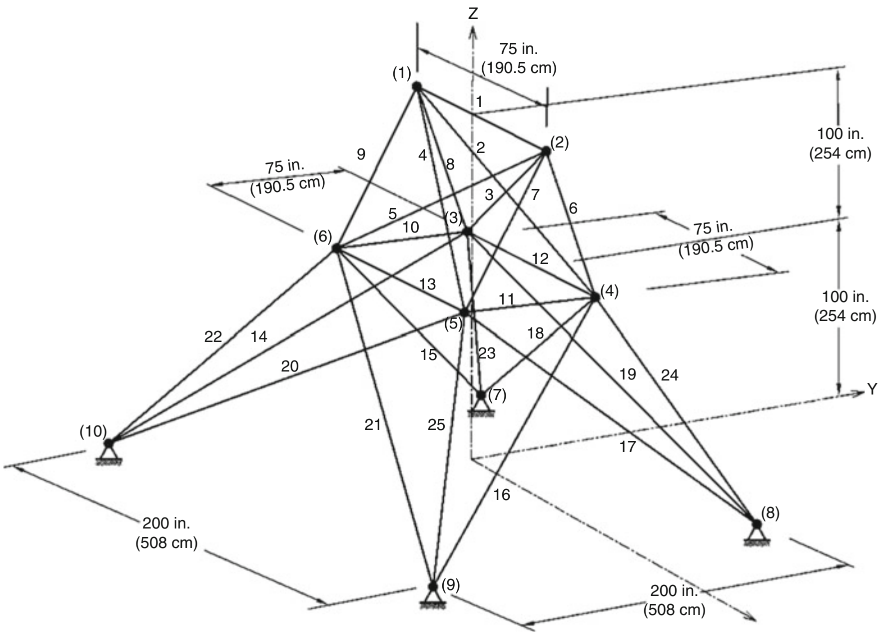

Fig. 7.12 Schematic of a 25-bar spatial truss

Table 7.9 Loading conditions for the 25-bar spatial truss

Node	Case 1			Case 2		
	P_X kips (kN)	P_Y kips (kN)	P_Z kips (kN)	P_X kips (kN)	P_Y kips (kN)	P_Z kips (kN)
1	0.0	20.0 (89)	−5.0 (22.5)	1.0 (4.45)	10.0 (44.5)	−5.0 (22.5)
2	0.0	−20.0 (89)	−5.0 (22.5)	0.0	10.0 (44.5)	−5.0 (22.5)
3	0.0	0.0	0.0	0.5 (22.5)	0.0	0.0
4	0.0	0.0	0.0	0.5 (22.5)	0.0	0.0

Table 7.10 Member stress limitations for the 25-bar spatial truss

Element group	Compressive stress limitations ksi (MPa)	Tensile stress limitation ksi (MPa)
1	35.092 (241.96)	40.0 (275.80)
2	11.590 (79.913)	40.0 (275.80)
3	17.305 (119.31)	40.0 (275.80)
4	35.092 (241.96)	40.0 (275.80)
5	35.092 (241.96)	40.0 (275.80)
6	6.759 (46.603)	40.0 (275.80)
7	6.959 (47.982)	40.0 (275.80)
8	11.082 (76.410)	40.0 (275.80)

Table 7.11 Comparison of CBO optimized designs with literature in the 25-bar spatial truss

Element group		Optimal cross-sectional areas (in^2)				
		Rajeev et al. GA [21]	Schutte et al. PSO [22]	Lee et al. HS [18]	Kaveh et al. RO [19]	Present work [2]
1	A_1	0.10	0.010	0.047	0.0157	0.0100
2	A_2–A_5	1.80	2.121	2.022	2.0217	2.1297
3	A_6–A_9	2.30	2.893	2.95	2.9319	2.8865
4	A_{10}–A_{11}	0.20	0.010	0.010	0.0102	0.0100
5	A_{12}–A_{13}	0.10	0.010	0.014	0.0109	0.0100
6	A_{14}–A_{17}	0.80	0.671	0.688	0.6563	0.6792
7	A_{18}–A_{21}	1.80	1.611	1.657	1.6793	1.6077
8	A_{22}–A_{25}	3.0	2.717	2.663	2.7163	2.6927
Best weight (Ib)		546	545.21	544.38	544.656	544.310
Average weight (Ib)		N/A	546.84	N/A	546.689	545.256
Std dev		N/A	1.478	N/A	1.612	0.294
No. of analyses		N/A	9596	15,000	13,880	9090

7.3.2.2 A 72-Bar Spatial Truss Structure

Schematic topology and element numbering of a 72-bar space truss are shown in Fig. 7.14. The elements are classified in 16 design groups according to Table 7.12.

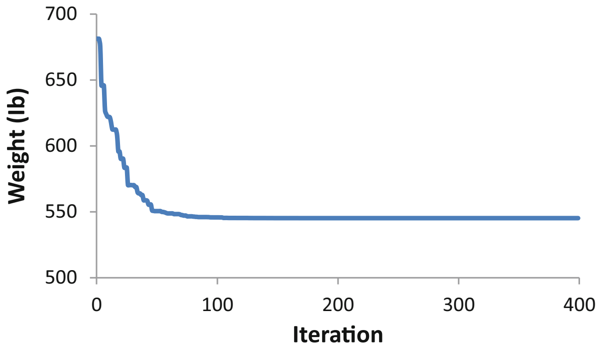

Fig. 7.13 The convergence diagram for the 25-bar spatial truss [2]

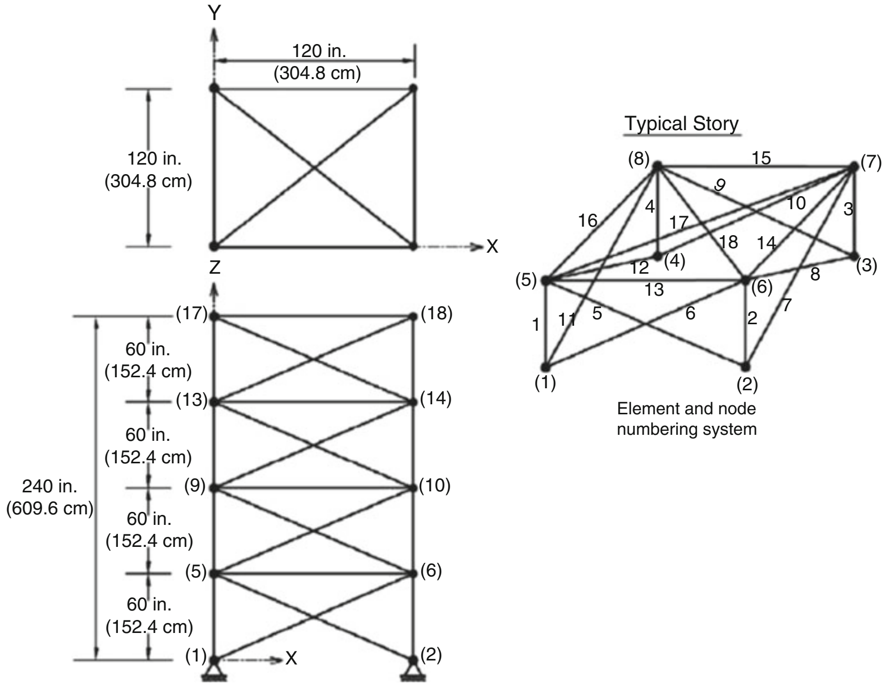

Fig. 7.14 Schematic of a 72-bar spatial truss

The material density is 0.1 lb/in^3 (2767.990 kg/m^3) and the modulus of elasticity is taken as 10,000 ksi (68,950 MPa). The members are subjected to the stress limits of ±25 ksi (±172.375 MPa). The uppermost nodes are subjected to the displacement limits of ±0.25 in (±0.635 cm) in both x and y directions. The minimum permitted cross-sectional area of each member is taken as 0.10 in^2 (0.6452 cm^2), and the

Table 7.12 Comparison of CBO optimized designs with literature in the 72-bar spatial truss (in^2)

Element group	Optimal cross-sectional areas (in^2)					
	Erbatur et al. GA [23]	Camp et al. ACO [24]	Perez et al. PSO [25]	Camp BB–BC [26]	Kaveh et al. RO [19]	Present work [2]
1–4	1.755	1.948	1.7427	1.8577	1.8365	1.9028
5–12	00.505	0.508	0.5185	0.5059	0.5021	0.5180
13–16	0.105	0.101	0.1000	0.1000	0.1000	0.1001
17–18	0.155	0.102	0.1000	0.1000	0.1004	0.1003
19–22	1.155	1.303	1.3079	1.2476	1.2522	1.2787
23–30	0.585	0.511	0.5193	0.5269	0.5033	0.5074
31–34	0.100	0.101	0.1000	0.1000	0.1002	0.1003
35–36	0.100	0.100	0.1000	0.1012	0.1001	0.1003
37–40	0.460	0.561	0.5142	0.5209	0.5730	0.5240
41–48	0.530	0.492	0.5464	0.5172	0.5499	0.5150
49–52	0.120	0.1	0.1000	0.1004	0.1004	0.1002
53–54	0.165	0.107	0.1095	0.1005	0.1001	0.1015
55–58	0.155	0.156	0.1615	0.1565	0.1576	0.1564
59–66	0.535	0.550	0.5092	0.5507	0.5222	0.5494
67–70	0.480	0.390	0.4967	0.3922	0.4356	0.4029
71–72	0.520	0.592	0.5619	0.5922	0.5971	0.5504
Best weight (Ib)	385.76	380.24	381.91	379.85	380.458	379.6943
Average weight (Ib)	N/A	383.16	N/A	382.08	382.553	379.8961
Std dev	N/A	3.66	N/A	1.912	1.221	0.0791
No. of analyses	N/A	18,500	N/A	19,621	19,084	15,600

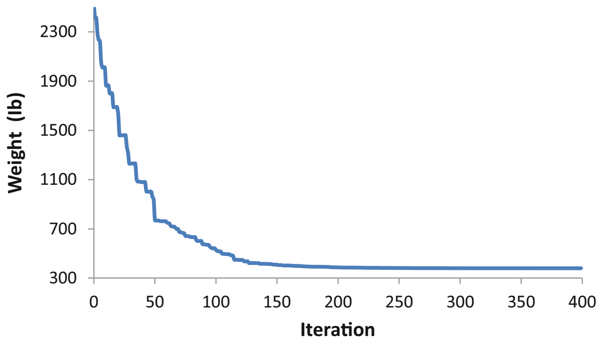

Fig. 7.15 The convergence diagram of the CBO algorithm for the 72-bar spatial truss [2]

maximum cross-sectional area of each member is 4.00 in^2 (25.81 cm^2). The loading conditions are considered as:

1. Loads 5, 5, and -5 kips in the x, y, *and* z directions at node 17, respectively
2. A load -5 kips in the z direction at nodes 17, 18, 19, and 20

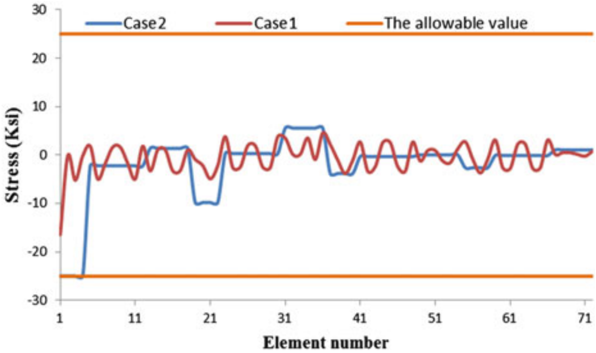

Fig. 7.16 Comparison of the allowable and existing stresses in the elements of the 72-bar truss structure [2]

Table 7.12 summarizes the results obtained by the present work and those of the previously reported researches. The best result of the CBO approach is 379.694, while it is 385.76, 380.24, 381.91, 379.85, and 380.458 *Ib* for the GA [23], ACO [24], PSO [25], BB–BC [26], and RO [19] algorithm, respectively. Also, the number of analyses of the CBO is 15,600, while it is 18,500, 19,621, and 19,084 for the ACO, BB–BC, and RO algorithm, respectively. Also, it is evident in Table 7.12 that the standard deviation of 20 independent runs for the CBO is less than the other optimization algorithms. Figure 7.15 shows the convergence diagrams in terms of the number of iterations for this example. Figure 7.16 shows the allowable and existing stress values in truss member using the CBO.

7.3.2.3 A 582-Bar Tower Truss

The 582-bar spatial truss structure, shown in Fig. 7.17, was studied with discrete variables by other researchers [27, 28]. However, here we have used this structure with continuous sizing variables. The 582 structural members categorized as 32 independent size variables. A single load case is considered consisting of lateral loads of 5.0 kN (1.12 kips) applied in both x and y directions and a vertical load of −30 kN (−6.74 kips) applied in the z direction at all nodes of the tower. The lower and upper bounds on size variables are taken as 3.1 in^2 (20 cm^2) and 155.0 in^2 (1000 cm^2), respectively.

The allowable tensile and compressive stresses are used as specified by the ASD-AISC [20] code, as Eqs. (7.28) and (7.29).

The maximum slenderness ratio is limited to 300 for tension members, and it is recommended to be limited to 200 for compression members according to ASD-AISC [20]. The modulus of elasticity is 29,000 ksi (203,893.6 MPa), and the yield stress of steel is taken as 36 ksi (253.1 MPa). Other constraints are the limitations of nodal displacements which should be no more than 8.0 cm (3.15 in.) in all directions.

Table 7.13 lists the optimal values of the 32 size variables obtained by the present algorithm. Figure 7.18 shows the convergence diagrams for the utilized

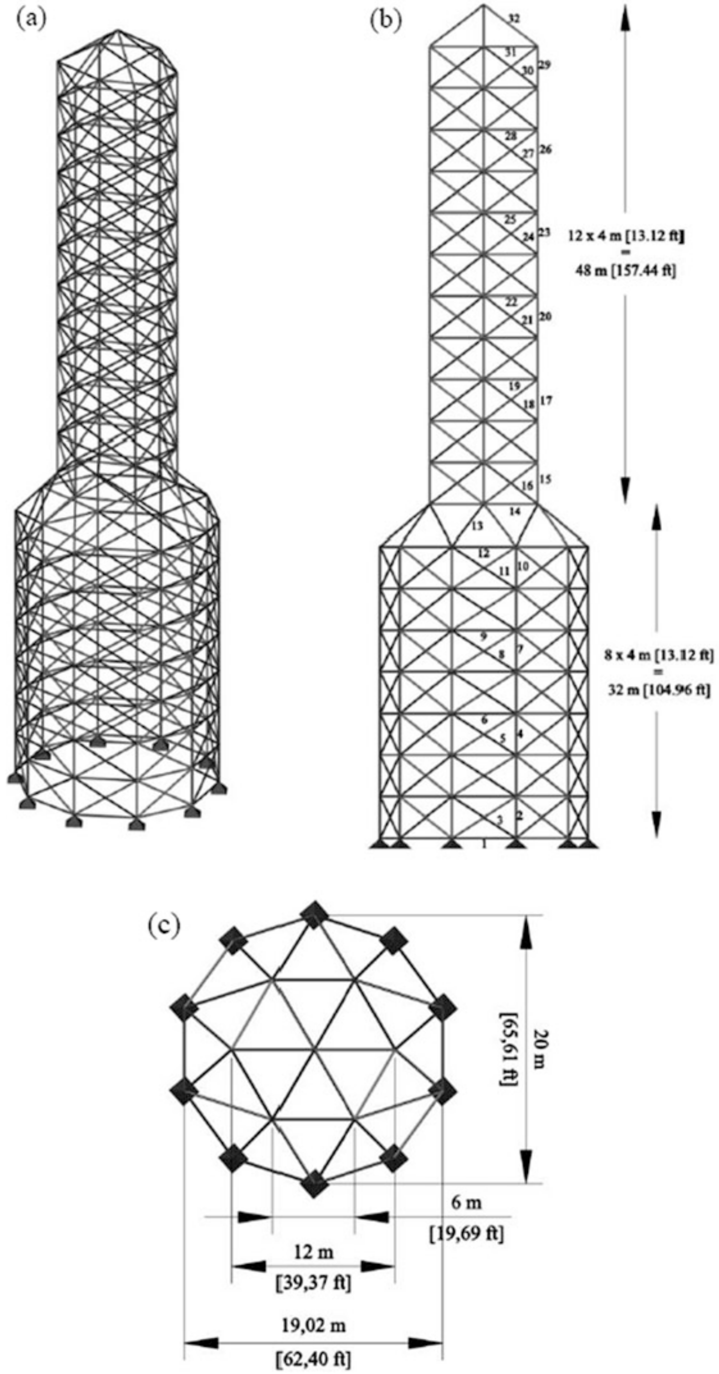

Fig. 7.17 Schematic of a 582-bar tower truss. (**a**) Three-dimensional view, (**b**) side view, (**c**) top view

Table 7.13 Optimum design cross sections for the 582-bar tower truss

Element groups	Present work [2] Area, cm^2	Element groups	Present work [2] Area, cm^2
1	20.5526	17	155.6601
2	162.7709	18	21.4951
3	24.8562	19	25.1163
4	122.7462	20	94.0228
5	21.6756	21	20.8041
6	21.4751	22	21.223
7	110.8568	23	53.5946
8	20.9355	24	20.628
9	23.1792	25	21.5057
10	109.6085	26	26.2735
11	21.2932	27	20.6069
12	156.2254	28	21.5076
13	159.3948	29	24.1394
14	107.3678	30	20.2735
15	171.915	31	21.1888
16	31.5471	32	29.6669
	Volume (m^3)		16.1520

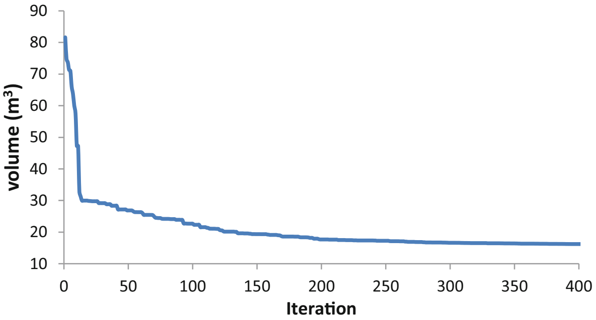

Fig. 7.18 The convergence diagram of the CBO for 582-bar tower truss [2]

algorithms. Figure 7.19 shows the allowable and existing stress ratio and displacement values of the CBO. Here, the number of structural analyses is taken as 20,000. The maximum values of displacements in the x, y, and z directions are 8 cm, 7.61 cm, and 2.15 cm, respectively. The maximum stress ratio is 0.47 %.

7.3.2.4 A 52-Bar Dome-Like Truss

Figure 7.20 shows the initial topology and the element numbering of a 52-bar dome-like space truss. This example has been investigated by Lingyun et al. [29]. Gomes [30] utilized the NHGA and PSO algorithms. This has also been

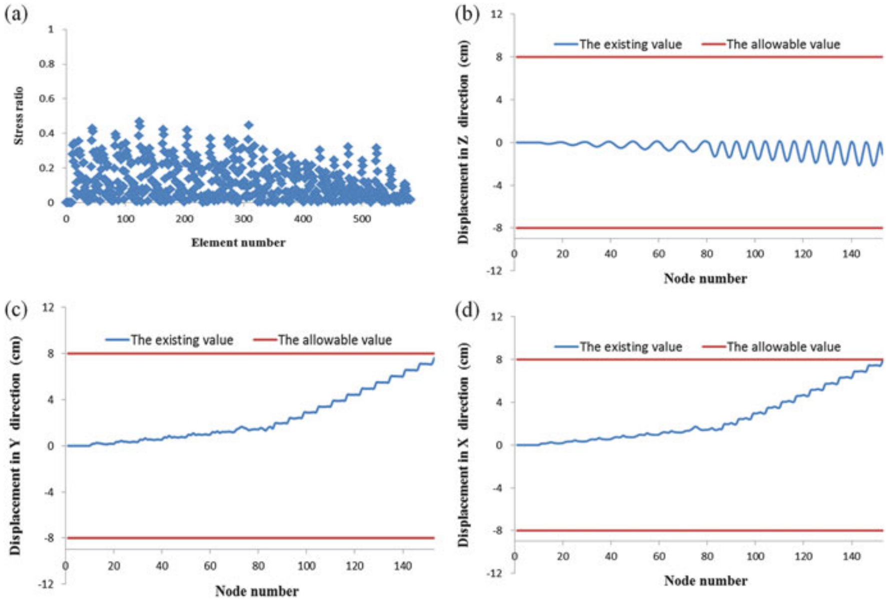

Fig. 7.19 Comparison of the allowable and existing constraints for the 582-bar truss using the DHPSACO, [2], (**a**) stress ratio, (**b**) displacement in the z direction. (**c**) Displacement in the y direction. (**d**). Displacement in the x direction

investigated by Kaveh and Zolghadr [31] using the standard CSS. This example is optimized for shape and configuration. The space truss has 52 bars, and nonstructural masses of $m = 50\,kg$ are added to the free nodes. The material density is $7800\,kg/m^3$ and the modulus of elasticity is $210,000\ \ MPa$. The structural members of this truss are categorized into eight groups, where all members in a group share the same material and cross-sectional properties. Table 7.14 shows each element group by member numbers. The range of the cross-sectional areas varies from 1 to 10 cm^2. The shape optimization is performed taking into account that the symmetry is preserved in the process of design. Each movable node is allowed to vary $\pm 2\,m$. There are two constraints in the first two natural frequencies so that $\omega_1 \leq 15.916\ HZ$ and $\omega_2 \geq 28.648\ HZ$. This example is considered to be a truss optimization problem with two natural frequency constraints and 13 design variables (five shape variables plus eight size variables).

Table 7.15 compares the cross section, best weight, mean weight, and standard deviation of 20 independent runs of CBO with the results of other researches. It is evident that the CBO is better than in terms of best weight of the results. Table 7.16 shows the natural frequencies of optimized structure obtained by different authors in the literature and the results obtained by the present algorithm. Figure 7.21 provides the convergence rates of the best result founded by the CBO.

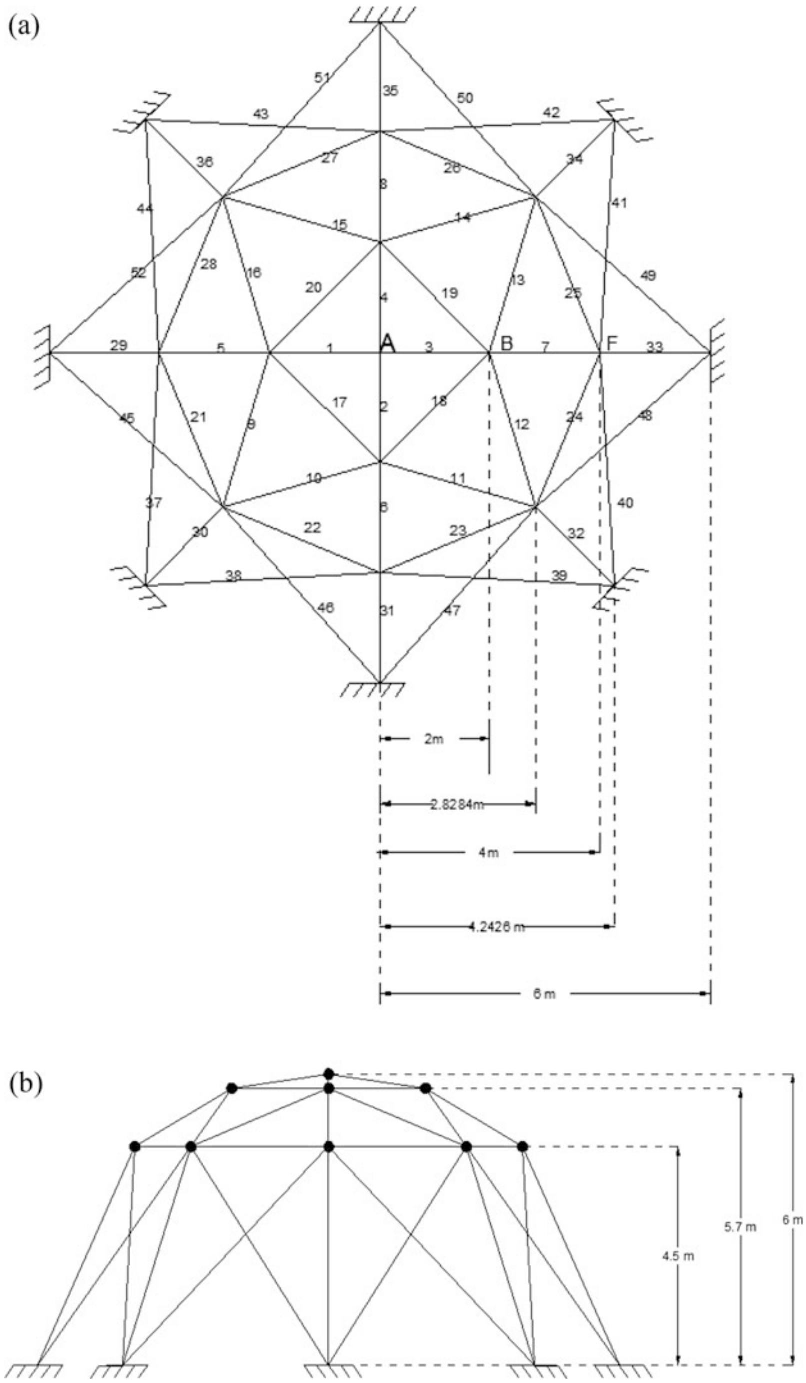

Fig. 7.20 Schematic of the 52-bar space truss. (**a**) Top view, (**b**) side view

Table 7.14 Element grouping

Group number	Elements
1	1–4
2	5–8
3	9–16
4	17–20
5	21–28
6	29–36
7	37–44
8	45–52

Table 7.15 Cross-sectional areas and nodal coordinates obtained by different researchers for the 52-bar space truss

Variable	Initial	Lingyun et al. GA [29]	Gomes PSO [30]	Kaveh et al. CSS [31]	Present work [2]
Z_A (*m*)	6.000	5.8851	5.5344	5.2716	5.6523
X_B (*m*)	2.000	1.7623	2.0885	1.5909	1.9665
Z_B (*m*)	5.700	4.4091	3.9283	3.7039	3.7378
X_F (*m*)	4.000	3.4406	4.0255	3.5595	3.7620
Z_F (*m*)	4.500	3.1874	2.4575	2.5757	2.5741
A_1 (cm^2)	2.0	1.0000	0.3696	1.0464	1.0009
A_2 (cm^2)	2.0	2.1417	4.1912	1.7295	1.3326
A_3 (cm^2)	2.0	1.4858	1.5123	1.6507	1.3751
A_4 (cm^2)	2.0	1.4018	1.5620	1.5059	1.6327
A_5 (cm^2)	2.0	1.9110	1.9154	1.7210	1.5521
A_6 (cm^2)	2.0	1.0109	1.1315	1.0020	1.0000
A_7 (cm^2)	2.0	1.4693	1.8233	1.7415	1.6071
A_8 (cm^2)	2.0	2.1411	1.0904	1.2555	1.3354
Best weight (*kg*)	338.69	236.046	228.381	205.237	197.962
Average weight (kg)	–	–	234.3	213.101	206.858
Std dev	–	–	5.22	7.391	5.750
No. of analyses	–	–	11,270	4000	4000

Table 7.16 Natural frequencies (*HZ*) of the optimized 52-bar planar truss

Frequency number	Initial	Lingyun et al. GA [29]	Gomes PSO [30]	Kaveh et al. CSS [31]	Present work [2]
1	22.69	12.81	12.751	9.246	10.2404
2	25.17	28.65	28.649	28.648	28.6482
3	25.17	28.65	28.649	28.699	28.6504
4	31.52	29.54	28.803	28.735	28.7117
5	33.80	30.24	29.230	29.223	29.2045

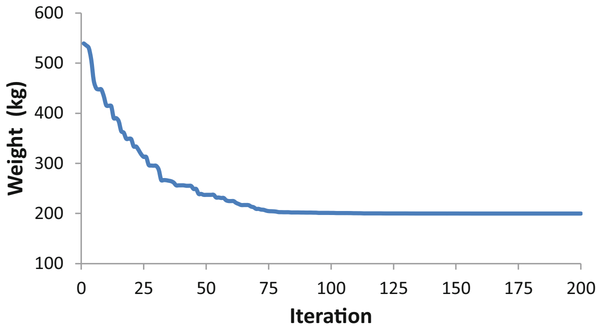

Fig. 7.21 Convergence history for the 52-bar truss [2]

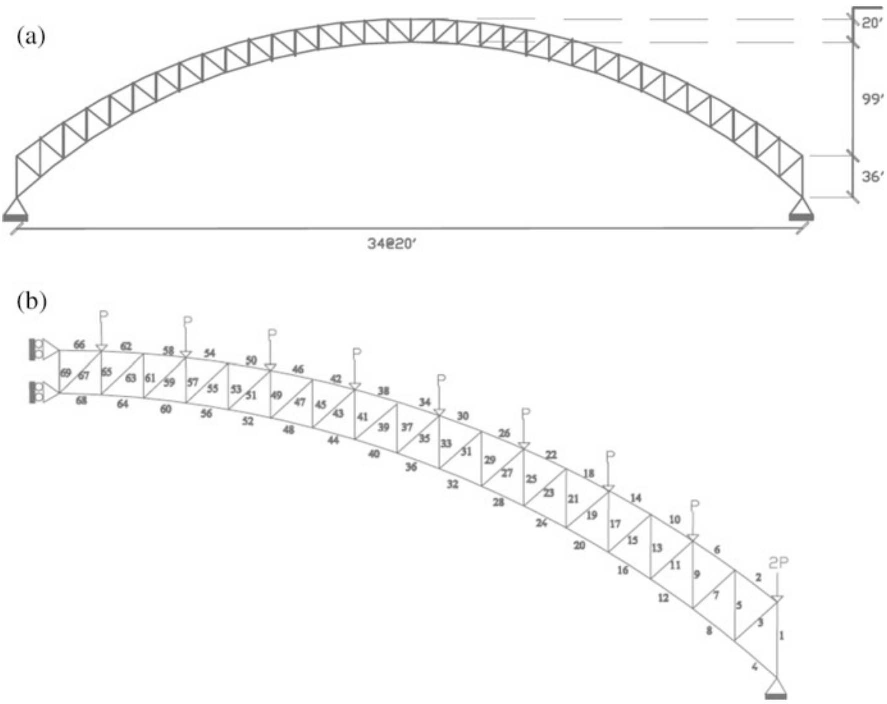

Fig. 7.22 (**a**) Schematic of the Burro Creek Bridge. (**b**) Finite element nodal and element numbering of Burro Creek Bridge

7.3.2.5 The Model of Burro Creek Bridge

The last example is the sizing optimization of the planar bridge shown in Fig. 7.22a. This example has been first investigated by Makiabadi et al. [32] using the teaching–learning-based optimization algorithm. This bridge is 680 ft long and 155 ft high truss of the main span. Also, both upper and lower chords shapes are

Table 7.17 Three different design variables for the Burro Creek Bridge

Design variables	Member number		
	Case 1 (4 variables)	Case 2 (8 variables)	Case 3 (12 variables)
1	67,63,59,55,51,47,43,39,35, 31,27,23,19,15,11,7,3	67,63,59,55,51,47,43,39,35, 31,27	67,63,59,55,51,47,43
2	66,62,58,54,50,46,42,38,34, 30,26,22,18,14,10,6,2	66,62,58,54,50,46,42,38,34, 30,26	66,62,58,54,50,46,42
3	69,65,61,57,53,49,45,41,37, 33,29,25,21,17,13,9,5,1	69,65,61,57,53,49,45,41,37, 33,29	69,65,61,57,53,49,45
4	68,64,60,56,52,48,44,40,36, 32,28,24,20,16,12,8,4	68,64,60,56,52,48,44,40,36, 32,28	68,64,60,56,52,48,44
5		23,19,15,11,7,3	39,35,31,27,23,19
6		22,18,14,10,6,2	38,34,30,26,22,18
7		25,21,17,13,9,5,1	41,37,33,29,25,21
8		24,20,16,12,8,4	40,36,32,28,24,20
9			15,11,7,3
10			14,10,6,2
11			17,13,9,5,1
12			16,12,8,4

Table 7.18 Comparison of CBO optimized cross-sectional areas (in^2) with those of TLS for the Burro Creek Bridge

Design variables	Maktobi et al. TLS [32]			Present work [2]		
	Case 1	Case 2	Case 3	Case 1	Case 2	Case 3
1	0.20000	0.2000	0.20000	0.20000	0.20000	0.20010
2	0.39202	0.46247	0.49843	0.35830	0.46532	0.43580
3	0.41654	0.22233	0.20000	0.20000	0.20007	0.20020
4	0.85487	0.57067	0.39476	0.78100	0.48657	0.32630
5		0.20012	0.20000		0.20000	0.20000
6		0.31227	0.42170		0.20004	0.27960
7		0.42791	0.25346		0.20001	0.20010
8		0.84160	0.63739		0.81310	0.70410
9			0.20000			0.20000
10			0.27992			0.20010
11			0.43354			0.20000
12			0.83483			0.74470
Best weight (Ib)	368,598.1	315,885.7	298,699.9	299,756.7	269,839.5	253,871.3
No. of analyses	15,000	35,000	50,000	8000	8000	8000

quadratic parabola. Because of symmetry of this truss, one can analyze half of the structure, Fig. 7.22b. The element groups and applied equivalent centralized loads are shown in Fig. 7.22b. The modulus of elasticity of material is $4.2 \times 10^9\ lb/ft^2$, Fy is taken as $72.0 \times 10^5\ lb/ft^2$, and the density of material is $495\ lb/ft^3$. For this

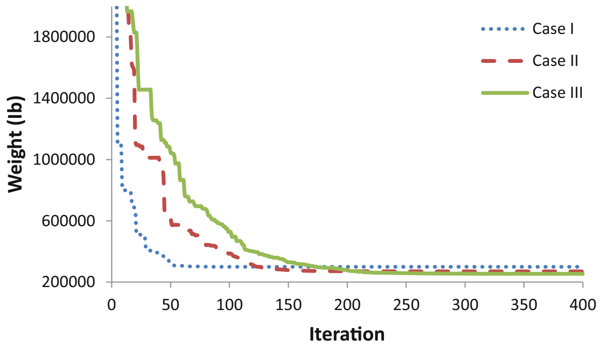

Fig. 7.23 Comparison of the convergence rates between three different cases for the Burro Creek Bridge [2]

example, allowable tensile and compressive stresses are considered according to ASD-AISC (1989) [20]. According to the Australian Bridge Code [33], the allowable displacement is 0.85 ft.

Three design cases are studied according to three different groups of variables including 4, 8, and 12 variables in the design. For three cases, the size variables are chosen from 0.2 to 5.0 in^2. Table 7.17 shows the full list of three different groups of variables used in the problem.

Table 7.18 compares the results obtained of the CBO with those of the TLS algorithm. The optimum weights of the CBO are 299,756.7, 269,839.5, and 253,871.3 Ib, while these are 368,598.1, 315,885.7, and 298,699.9 for Cases 1, 2, and 3, respectively. It can be seen that the number of analyses is much less than that of TLS algorithm. Figure 7.23 provides a comparison of the convergence diagrams of the CBO for three cases.

7.3.3 Discussion

CBO utilizes a simple formulation to find minimum of functions and does not depend on any internal parameter. Also, the formulation of CBO algorithm does not use the memory for saving the best-so-far solution (i.e., the best position of agents from the previous iterations). By defining the coefficient of restitution (COR), a good balance between the global and local search is achieved in CBO. The proposed approach performs well in several test problems both in terms of the number of fitness function evaluations and in terms of the quality of the solutions. The results are compared to those generated with other techniques reported in the literature.

References

1. Kaveh A, Mahdavi VR (2014) Colliding bodies optimization: a novel meta-heuristic method. Comput Struct 139:18–27
2. Kaveh A, Mahdavi VR (2014) Colliding bodies optimization method for optimum design of truss structures with continuous variables. Adv Eng Softw 70:1–12
3. Tolman RC (1979) The principles of statistical mechanics. Clarendon Press, Oxford (Reissued)
4. Tsoulos IG (2008) Modifications of real code genetic algorithm for global optimization. Appl Math Comput 203:598–607
5. Coello CAC (2000) Use of a self-adaptive penalty approach for engineering optimization problems. Comput Ind 41:113–127
6. He Q, Wang L (2007) An effective co-evolutionary particle swarm optimization for constrained engineering design problem. Eng Appl Artif Intell 20:89–99
7. Montes EM, Coello CAC (2008) An empirical study about the usefulness of evolution strategies to solve constrained optimization problems. Int J Gen Syst 37:443–473
8. Kaveh A, Talatahari S (2010) A novel heuristic optimization method: charged system search. Acta Mech 213:267–289
9. Ragsdell KM, Phillips DT (1976) Optimal design of a class of welded structures using geometric programming. ASME J Eng Ind Ser B 98:1021–1025
10. Deb K (1991) Optimal design of a welded beam via genetic algorithms. AIAA J 29:2013–2015
11. Coello CAC, Montes EM (1992) Constraint-handling in genetic algorithms through the use of dominance-based tournament. IEEE Trans Reliab 41(4):576–582
12. Sandgren E (1988) Nonlinear integer and discrete programming in mechanical design. In: Proceedings of the ASME design technology conference, Kissimine, FL, pp 95–105
13. Kannan BK, Kramer SN (1994) An augmented Lagrange multiplier based method for mixed integer discrete continuous optimization and its applications to mechanical design. Trans ASME J Mech Des 116:318–320
14. Deb K, Gene AS (1997) A robust optimal design technique for mechanical component design. In: Dasgupta D, Michalewicz Z (eds) Evolutionary algorithms in engineering applications. Springer, Berlin, pp 497–514
15. Belegundu AD (1982) A study of mathematical programming methods for structural optimization. Ph.D. thesis, Department of Civil and Environmental Engineering, University of Iowa, Iowa, USA
16. Arora JS (1989) Introduction to optimum design. McGraw-Hill, New York
17. Soh CK, Yang J (1996) Fuzzy controlled genetic algorithm search for shape optimization. J Comput Civil Eng ASCE 10:143–150
18. Lee KS, Geem ZW (2004) A new structural optimization method based on the harmony search algorithm. Comput Struct 82:781–798
19. Kaveh A, Khayatazad M (2012) A novel meta-heuristic method: ray optimization. Comput Struct 112–113:283–294
20. American Institute of Steel Construction (AISC) (1989) Manual of steel construction—allowable stress design, 9th edn. AISC, Chicago, IL
21. Rajeev S, Krishnamoorthy CS (1992) Discrete optimization of structures using genetic algorithms. Struct Eng ASCE 118:1233–1250
22. Schutte JJ, Groenwold AA (2003) Sizing design of truss structures using particle swarms. Struct Multidiscip Optim 25:261–269
23. Erbatur F, Hasançebi O, Tütüncü I, Kiliç H (2000) Optimal design of planar and space structures with genetic algorithms. Comput Struct 75:209–224
24. Camp CV, Bichon J (2004) Design of space trusses using ant colony optimization. J Struct Eng ASCE 130:741–751
25. Perez RE, Behdinan K (2007) Particle swarm approach for structural design optimization. Comput Struct 85:1579–1588

26. Camp CV (2007) Design of space trusses using Big Bang–Big Crunch optimization. J Struct Eng ASCE 133:999–1008
27. Kaveh A, Talatahari S (2009) A particle swarm ant colony optimization for truss structures with discrete variables. J Constr Steel Res 65:1558–1568
28. Hasançebi O, Çarbas S, Dogan E, Erdal F, Saka MP (2009) Performance evaluation of metaheuristic search techniques in the optimum design of real size pin jointed structures. Comput Struct 87:284–302
29. Lingyun W, Mei Z, Guangming W, Guang M (2005) Truss optimization on shape and sizing with frequency constraints based on genetic algorithm. J Comput Mech 25:361–368
30. Gomes MH (2011) Truss optimization with dynamic constraints using a particle swarm algorithm. Expert Syst Appl 38:957–968
31. Kaveh A, Zolghadr A (2011) Shape and size optimization of truss structures with frequency constraints using enhanced charged system search algorithm. Asian J Civil Eng 12:487–509
32. Makiabadi MH, Baghlani A, Rahnema H, Hadianfard MA (2013) Optimal design of truss bridges using teaching–learning-base optimization algorithm. Int J Optim Civil Eng 3 (3):499–510
33. AustRoads. 92 (1992) Austroads bridge design code. Australasian Railway Association, NSW